Nitroxide Radicals@US-Tubes: New Spin Labels for Biomedical Applications

*Eladio J. Rivera, Richa Sethi, Feifei Qu, Ramkumar Krishnamurthy, Raja Muthupillai, Michael Alford, Michael A. Swanson, Sandra S. Eaton, Gareth R. Eaton, and Lon J. Wilson**

The encapsulation of nitroxide radicals within ultrashort (ca. 50 nm) single-walled carbon nanotubes (US-tubes) is achieved. Tempo- and Iodo-Tempo@US-tubes are characterized by thermogravimetric analysis (TGA), X-ray photoelectron spectroscopy (XPS), and Raman spectroscopy. Electron paramagnetic resonance (EPR) spectra display characteristic signals due to the detection of the spin probes within the US-tubes. Longitudinal proton relaxivities (r_1) of both nitroxide@US-tubes samples are 7 to 13 times greater than the free nitroxide radicals in solution, giving relaxivities comparable to the clinical contrast agent (CA) Magnevist. In addition, transverse proton relaxivities (r_2) show unprecedented proton relaxation enhancement in comparison to any other reported nitroxide radical-based system or the clinically approved T_2 CA, Resovist, under the same conditions. T_2-weighted magnetic resonance imaging (MRI) phantom images show that the encapsulation of nitroxide radicals within the US-tubes produces good contrast enhancement due to their high r_2 relaxivities. The nitroxide radicals@US-tube agents are a new promising class of spin probes for MRI and electronic paramagnetic resonance imaging (EPRI) labeling, tracking, and diagnosis.

1. Introduction

Magnetic resonance imaging (MRI) is one of the most powerful and non-invasive diagnostic techniques for living organisms based on the interaction of the nuclear magnetic moment of water protons in tissues with an external magnetic field. The signal intensity in MRI depends upon the relaxation rates of the water protons. MRI images can be improved by administering paramagnetic agents which increase the longitudinal relaxation rates of nearby water protons, thereby enhancing the MRI signal.[1] Gadolinium complexes with paramagnetic Gd^{3+} ions are the most clinically-used commercial contrast agents (CAs) because of their seven unpaired electrons ($S = 7/2$) and long electronic relaxation time.[2] However, the short blood circulation time and non-specific biodistribution of these CAs are limitations of such agents. The measure of signal enhancement due to MRI CAs is described by the term relaxivity, defined as the change in the relaxation rate of the water protons per mM concentration of the CA. Gadolinium-based CAs increase both the longitudinal (T_1^{-1}) and transverse (T_2^{-1}) relaxation rates of nearby water protons, thereby improving the contrast in T_1- and T_2-weighted images.[2]

Nitroxide radicals are non-toxic, stable, organic free radicals having a single unpaired electron ($S = 1/2$) which are therefore capable of providing MRI contrast by shortening the proton longitudinal relaxation time (T_1). Since 1984, nitroxide radicals have been studied as both MRI CAs[3,4] and electron paramagnetic resonance imaging (EPRI) agents.[5,6] They have long been utilized as biophysical tools for EPR spectroscopic studies such as spin label oximetry and spin trapping because of their stability and paramagnetism.[7] In addition, nitroxide radicals have shown excellent cell and blood-brain barrier (BBB) permeability and are therefore more amenable for in vivo use than Gd^{3+}-ion complexes.[8,9] Other applications such as in vivo EPRI,[8,10] radioprotection,[11] and noninvasive assessment of tissue redox status[12] have been reported recently. Nitroxide radicals have much smaller longitudinal relaxivity ~0.2 $mM^{-1}s^{-1}$ when compared to Gd^{3+}-ion complexes in MRI,[3,13–15] but at the same time, they have advantages due to their lower toxicity in comparison with Gd^{3+} ion and the emergance of methods for circumventing the in vivo nitroxide reduction problem.[16,17] In principle, it also may be possible

E. J. Rivera, R. Sethi, Prof. L. J. Wilson
Department of Chemistry MS-60
Smalley Institute for Nanoscale Science and Technology
P. O. Box 1892 Rice University,
Houston TX 77251-1892, USA
E-mail: durango@rice.edu
F. Qu, R. Krishnamurthy, R. Muthupillai
Department of Radiology
St. Luke's Episcopal Hospital
6720 Bertner Avenue, MC 2-270, Houston, TX 77030-2697, USA
M. Alford
TDA Research Inc.
12345 W. 52nd Avenue, Wheat Ridge, CO 80033, USA
M. A. Swanson, Prof. S. S. Eaton, Prof. G. R. Eaton
Department of Chemistry and Biochemistry
University of Denver
2101 E. Wesley Avenue, Denver, CO 80208, USA

DOI: 10.1002/adfm.201102826

to make nitroxide radicals more effective CAs by placing them in chemical structures which effectively force water molecules into close proximity to the nitroxide group, thereby greatly enhancing the water proton relaxation rates.[18] Different systems have been reported that involve the encapsulation or functionalization of nitroxide radicals into calix[4]arenes,[19] polymers,[20–22] anticancer drugs,[8] dendrimers,[23,24] and biomolecules such as DNA oligomers,[25] liposomes,[26] human serum albumin[27]; however, limited success has been achieved in enhancing proton relaxivity and tissue targeting capability. It is possible that carbon nanotubes (CNTs), and more specifically ultra-short carbon nanotubes (US-tubes) derived from single-walled carbon nanotubes (SWNTs), have the potential to overcome these limitations for nitroxide radical CAs in a manner similar to that for encapsulation of Gd^{3+} ions within US-tubes that produced the high-performance MRI CAs called gadonanotubes (GNTs).[28]

SWNTs have many unique mechanical, electronic, and optical properties that are potentially useful in medicine, and there is currently an intense research effort to develop biomedical applications for these materials, particularly for the treatment and diagnosis of cancer.[29,30] The EPR characterization of CNT materials containing encapsulated nitroxide radicals have recently been reported.[1,31,32] These investigations have involved the use of spin probes in an effort to better understand the environment in the CNT, however, application of these systems for MRI, EPRI, and oximetry has not been previously explored. In particular, US-tubes offer a convenient platform for encapsulating metal ions and small molecules, and potentially targeting them for biomedical applications with exterior sidewall derivatizations.[33–35] In fact, we have previously used US-tubes to successfully encapsulate different materials of medical interest such as cisplatin to prepare smart drug delivery systems,[36] I_2 molecules for an X-ray contrast agent,[37] ^{211}AtCl molecules for α-radiotheraphy,[38] and Gd^{3+} ions to produce the GNTs as a new high-performance MRI CA.[28,39] Taking advantage of this previous work, we now propose to utilize US-tubes to encapsulate and transport nitroxide radicals spin probes for biological applications such as MRI and EPRI.

2. Results and Discussion

2.1. Characterization of Tempo- and Iodo-Tempo@US-Tubes

The nitroxide radicals@US-tube materials are nanoscale CNT capsules (derived from full-length SWNTs) with a length of 20–80 nm and diameter of ~ 1.4 nm, which are internally loaded with Tempo and Iodo-Tempo as spin probes. **Figure 1**a shows the chemical structures of Tempo and Iodo-Tempo and Figure 1b displays a structural depiction of a US-tube loaded with a single Tempo molecule. Nitroxide radical loading may occur through the sidewall defects or the end of tube openings created during the SWNT cutting procedure (see Experimental Section). The concentration of the nitroxide radicals inside the US-tubes was determined by elemental analysis for N (Tempo@US-tubes: C 67.11%, N 0.77%, H 1.98%; Iodo-Tempo@US-tubes: C 51.28%, N 1.09%, H 1.69%) performed by a commercial laboratory (Galbraith Laboratories, Inc., Nashville, Tenn., USA). Assuming that the average US-tube contains 120 carbons nm^{-1},[35,37] there are approximately 15 to 34 molecules of Iodo-Tempo and Tempo per US-tube, respectively. The preparation of the Tempo- and Iodo-Tempo@US-tubes was accomplished by sublimation of the nitroxide radical into US-tubes in a closed glass vessel for 24 h (see Experimental Section). The obtained materials were characterized by TGA, XPS, and Raman spectroscopy.

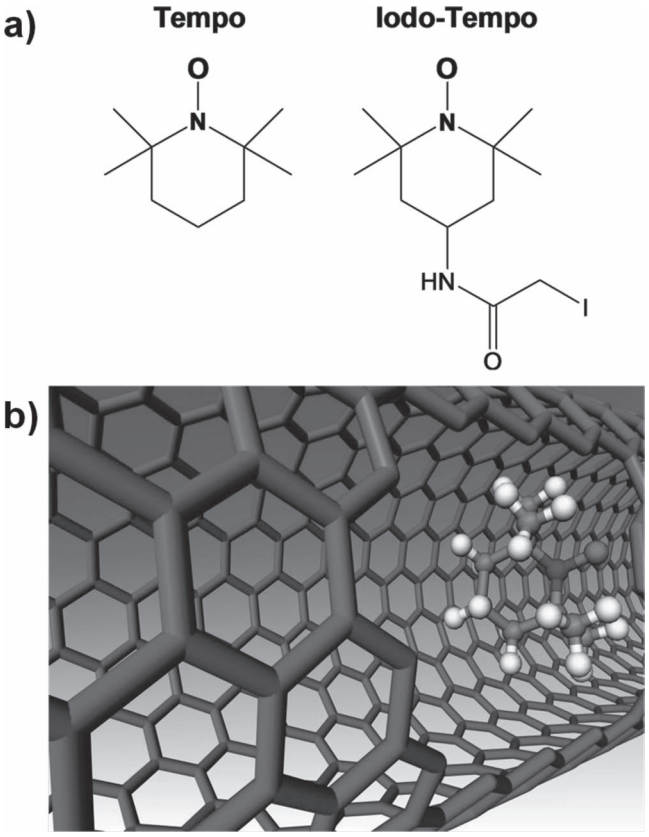

Figure 1. a) Tempo and Iodo-Tempo nitroxide radical chemical structures. b) Depiction of a US-tube loaded with a single Tempo molecule.

Figure 2a,b show the TGA curves of US-tubes, nitroxide radicals, and Tempo- and Iodo-Tempo@US-tube samples under argon atmosphere. The US-tubes showed a 1% weight loss from 50-100 °C, probably due to a small amount of residual water in the samples and did not show any further weight loss until over 250 °C. Only a 12% weight loss was observed over the entire 250–800 °C range. TGA behavior of the Tempo and Iodo-Tempo nitroxide radicals showed that they sublime or decompose over 70–145 °C and 170-650 °C temperature ranges, respectively (insets in Figure 2a,b).[41,42] The Tempo- and Iodo-Tempo@US-tube samples displayed approximately 14% and 17% weight losses, respectively, suggesting the slow release/decomposition of the nitroxide radicals from the US-tube samples over a 250–650 °C range. Loss of any externally-absorbed nitroxide for the nitroxide@US-tube samples would have occurred by 150 °C for Tempo and by 350 °C for Iodo-Tempo (insets in Figure 2a,b), and no sharp weight loss before these temperatures was observed for either sample.

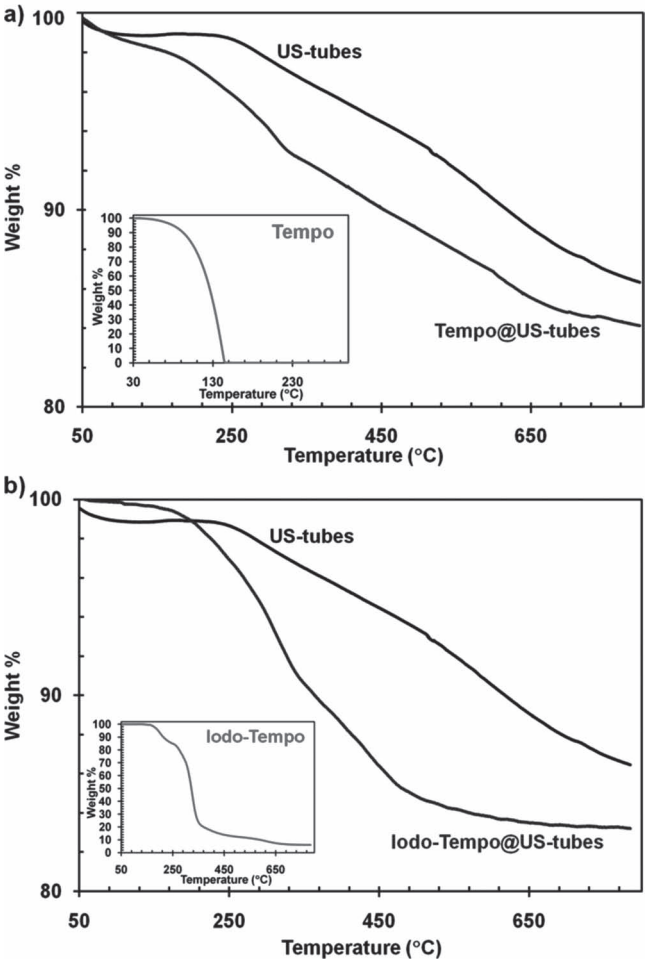

Figure 2. TGA curves of a) Tempo nitroxide radical (inset), US-tubes, and Tempo@US-tubes and b) Iodo-Tempo nitroxide radical (inset), US-tubes, and Iodo-Tempo@US-tubes under argon atmosphere.

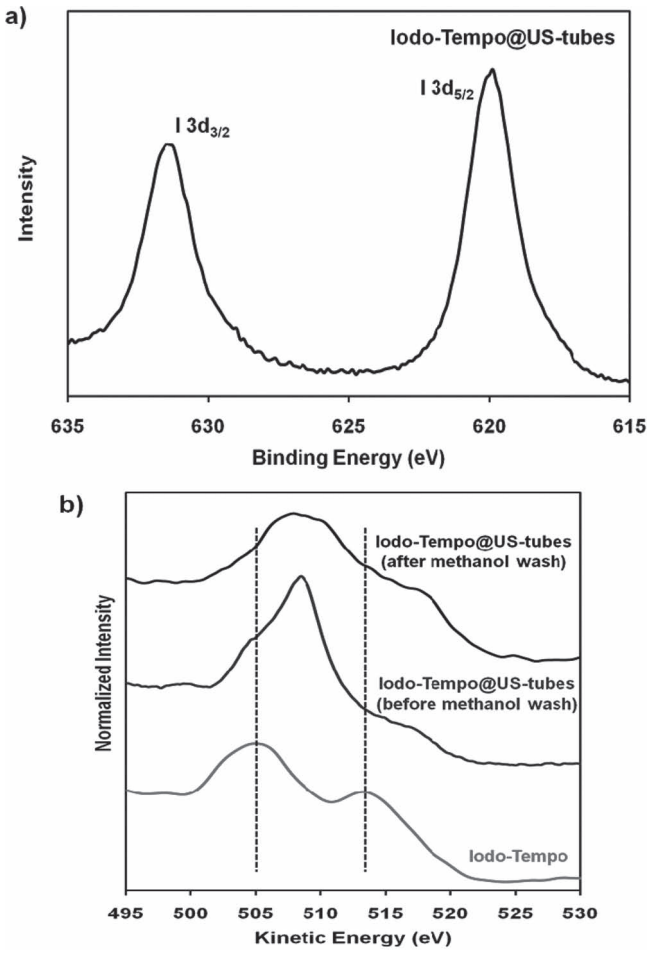

Figure 3. a) XPS spectrum of Iodo-Tempo@US-tubes over the I 3d binding region. b) Auger spectra over the I-MNN region for Iodo-Tempo and Iodo-Tempo@US-tubes after the sublimation process, followed by extensive washings with methanol.

XPS and Auger spectroscopy have been used to distinguish between externally-adsorbed and internally-loaded Iodo-Tempo molecules in the Iodo-Tempo@US-tube sample. A typical XPS spectrum of Tempo@US-tubes over the N 1s binding energy region is shown in Figure 1S of the Supporting Information. The XPS spectrum of Iodo-Tempo@US-tubes showed the I $3d_{5/2}$ and I $3d_{3/2}$ peaks at 619.9 and 631.5 eV binding energies, respectively, due to the presence of the iodine group of the nitroxide radical structure (**Figure 3**a). Figure 3b shows the Auger spectra for Iodo-Tempo nitroxide radical and Iodo-Tempo@US-tubes over the I-MNN region. The Iodo-Tempo nitroxide radical exhibits peaks at kinetic energies of 505.0 and 513.8 eV. After the sublimation process, the Iodo-Tempo@US-tube sample showed the appearance of a new intense peak at 508.7 eV, suggesting a different chemical environment for Iodo-Tempo in the presence of the US-tubes. Also, one of the characteristic peaks of Iodo-Tempo remained (505.0 eV), while the second peak was shifted to higher kinetic energy (515.8 eV), probably due to externally-adsorbed nitroxide. Finally, the Iodo-Tempo@US-tube sample washed with a large excess of methanol exhibited a peak at a kinetic energy of 509.0 eV and with a shoulder at 517.6 eV. These kinetic energies are in good agreement with previous reports of Auger I-$M_5N_{45}N_{45}$ and I-$M_4N_{45}N_{45}$ transitions for internally-loaded molecular iodine (I_2) within the US-tubes,[37,43] strongly suggesting that all the Iodo-Tempo in the Iodo-Tempo@US-tube sample is internally-loaded within the US-tubes.

Raman spectroscopy can show direct evidence for the interactions of the nitroxide radicals within the US-tubes. **Figure 4** and **5** show Raman spectra of the US-tube, Tempo@US-tube, and Iodo-Tempo@US-tube samples. The G-, D-, and radial breathing modes (RBM) of the US-tubes are shown to be sensitive to the encapsulation of the nitroxide radicals within the US-tubes. US-tubes displayed characteristic Raman peaks with radial breathing modes (RBM) at ~132, 145, and 156 cm^{-1}, and with D- and G- bands located at ~1,316 and 1,577 cm^{-1}, respectively.[40,44] As denoted by an asterisk in the Tempo- and Iodo-Tempo@US-tube spectra, the G-band showed the formation of a shoulder ~1,555 cm^{-1} (Figure 4b and 5b) and intense RBM sharp peaks at ~143, and 157 cm^{-1} (Figure 4c and 5c). A similar behavior was previously observed for other types of organic molecules encapsulated in SWNTs.[45,46]

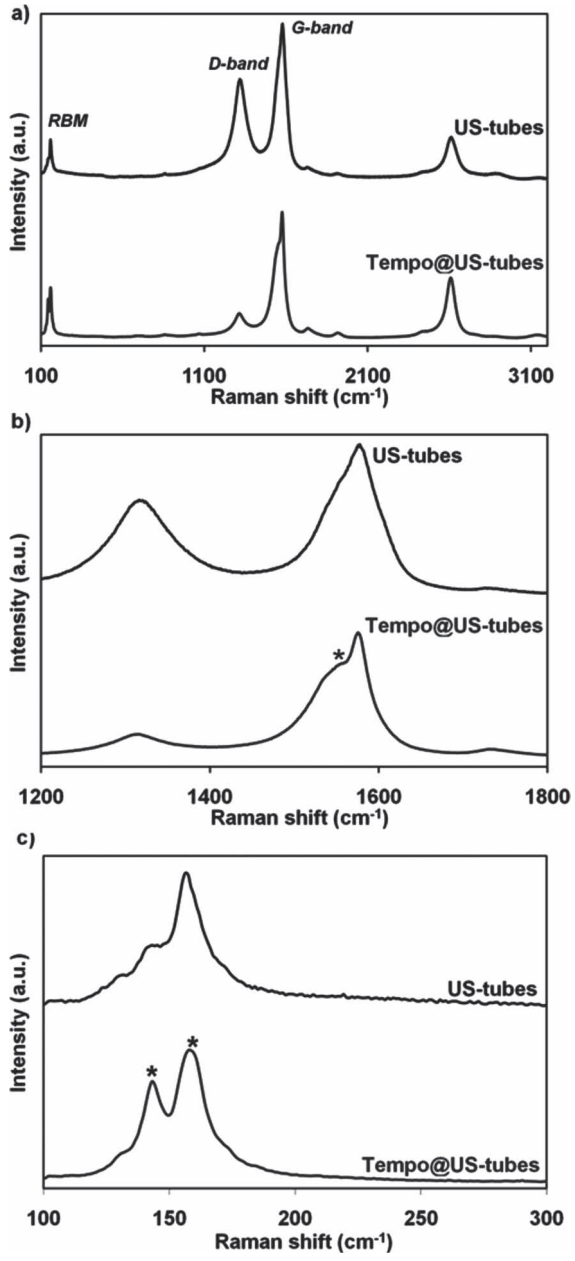

Figure 4. a) Complete Raman spectra of US-tubes and Tempo@US-tubes, b) the G- and D- bands region, and c) the RBM region. Spectral changes due to encapsulation of Tempo within US-tubes are denoted by asterisks.

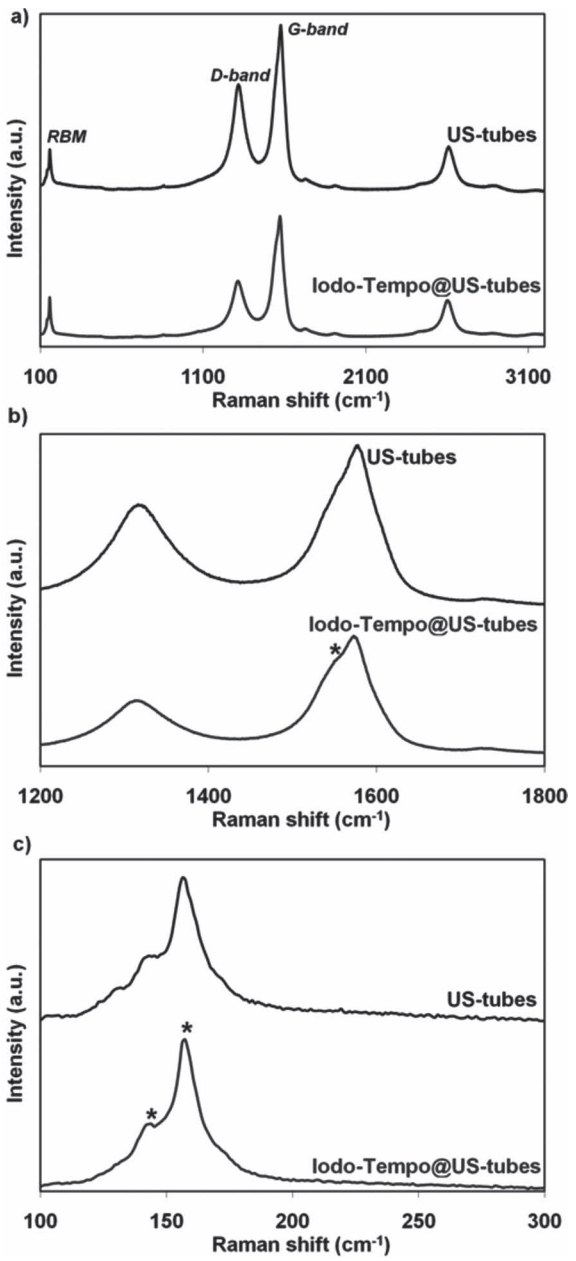

Figure 5. a) Complete Raman spectra of US-tubes and Iodo-Tempo@US-tubes, b) the G- and D- bands region, and c) the RBM region. Spectral changes due to encapsulation of Iodo-Tempo within US-tubes are denoted by asterisks.

2.2. EPR Spectroscopic Studies

Figure 6 shows the EPR spectra from powders of the empty US-tubes and nitroxide@US-tube samples. Wide (4000-G) scans of the EPR spectra of the US-tubes with or without nitroxides (Figure 6a–c) exhibit a strong broad signal with peak-to-peak linewidth of 650 G at about 3200 G (g ~ 2.2). This broad signal is attributed to magnetic metal catalyst impurities from the carbon arc-discharge SWNT production method.[47–49] To more clearly see signals in the vicinity of g ~ 2.00 that are characteristic of organic radicals, including nitroxides,[50] 200 G scans centered at 3519 G were recorded (see insets in Figure 6). For the empty US-tube sample, there is a weak signal with peak-to-peak linewidth of 4 G at g ~ 2.002 that is attributed to US-tube-centered organic radicals (inset in Figure 6a). For freely-tumbling nitroxides in solution, the EPR spectrum would consist of three narrow lines of equal intensity due to hyperfine interaction with the nitrogen nuclear spin (I = 1),[50,51] and the high concentration of nitroxide in the US-tubes would be expected to result in collisional broadening. The absence of a

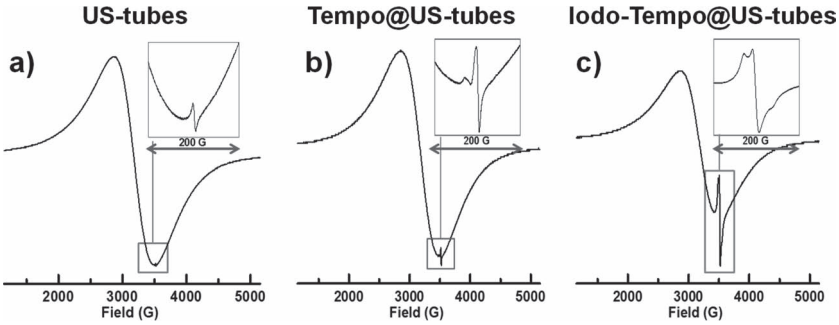

Figure 6. EPR spectra from powders of the empty US-tube and the nitroxide-labeled US-tube samples at room temperature.

sharp 3-line signal in the spectra of Tempo- and Iodo-Tempo@US-tubes (Figure 6b and 6c) indicates the absence of freely-tumbling nitroxide. Limited mobility of the nitroxides is attributed to interactions with the interior of the US-tubes. The EPR spectra of immobilized nitroxides are more complicated due to the anisotropy of the nitrogen hyperfine coupling. In the spectrum of Tempo@US-tubes (Figure 6b inset) the peaks at ~ 3492 and 3520 G and the broad shoulder at ~ 3553 G exhibit the splitting characteristic of an immobilized nitroxide. The larger intensity of the peak at ~3520 G that is typical for immobilized spectra may be due to an exchange narrowed component. In the spectrum of Iodo-Tempo@US-tubes (Figure 6c inset), the broadened signal from the immobilized nitroxide is consistent with electron-electron exchange interactions between the closely spaced nitroxides. Power saturation measurements of the nitroxyl EPR signal of Tempo@US-tubes show linearity up to approximately 15 mW (Figure 2S, Supporting Information). For an immobilized nitroxide at low concentration in a diamagnetic environment, the linear region of the power saturation curve would be expected to extend only to a few mW. The relaxation enhancement is consistent with significant interaction among nitroxides and the nitroxides with the paramagnetic species responsible for the broad EPR signal as expected when incorporated into the US-tubes.

2.3. Proton Relaxation Properties and Magnetic Resonance Imaging

The water proton relaxation times and relaxivities for Tempo- and Iodo-Tempo@US-tubes and empty US-tubes in 0.17% pluronic F-108 surfactant at 1.41 T and 37 ºC are given in **Table 1**. To compare the relaxation rate enhancement from the nitroxide radicals@US-tube samples, the relaxation rates of the free nitroxide radicals in solution were determined from the relaxation times as a function of concentration by using the inversion recovery method and multi-echo sequence (see Experimental Section and Figure 3S and 4S, Supporting Information). Linear regression analyses yielded relaxivities (r_1 and r_2) of 0.15 and 0.10 $mM^{-1}s^{-1}$ for Tempo and 0.27 and 0.43 $mM^{-1}s^{-1}$ for Iodo-Tempo radical, respectively. Comparing the relaxivities of the Tempo- and Iodo-Tempo@US-tubes (r_1 ~ 2 $mM^{-1}s^{-1}$) with the free nitroxide radicals and empty US-tubes, it is interesting to note that the r_1 of the nitroxide radicals@US-tube samples are 7–13 times greater than for free nitroxide radicals in solution and 20 times greater than for empty US-tubes. The r_1 values of the nitroxide radicals@US-tubes are comparable to clinically-used Gd-based CAs (r_1 ~ 4 $mM^{-1}s^{-1}$)[52] and exceed that of any other nitroxide radical-based system under the same conditions.[23,24] The r_2 relaxivities of the Iodo-Tempo- and Tempo@US-tubes (110 and 132 $mM^{-1}s^{-1}$, respectively) are 30 times greater than for empty US-tubes and a several-fold relaxation enhancement than for free nitroxide radicals in solution. The relaxivity ratios (r_2/ r_1) of Iodo-Tempo- and Tempo@US-tubes are therefore 30 to 90 times greater than the free nitroxide radicals, respectively. The r_2 values of the nitroxide radicals@US-tubes exceed that of carboxydextran-coated superparamagnetic iron nanoparticles (SPION) CA Resovist (r_2 ~ 82 $mM^{-1}s^{-1}$) and also approximately equal that of SPION-encapsulated micelles (PEG-PLC-SPIONs; r_2 ~ 121 $mM^{-1}s^{-1}$).[53]

To verify the effectiveness of the nitroxide radicals@US-tubes as CAs, we obtained T_1- and T_2-weighted MRI phantom images, as well as the T_1- and T_2-maps from the nitroxide radicals@US-tube and empty US-tube samples in 1% agarose gel. We deliberately used agarose gel in our phantom samples because it offers structural stability that closely matches the in vivo properties of tissue.[54] **Figure 7** shows the T_2-weighted MRI phantom images and the T_2 map of nitroxide radicals@US-tube and empty US-tube samples at 3.0 T in 1% agarose gel. It is important to note that the transverse (T_2) relaxation times from suspensions of the nitroxide radicals@US-tubes in 0.17% pluronic F-108 measured in the MRI scanner (data not shown) are in good agreement with the results obtained using the Bruker Minispec NMR spectrometer. However, when we immobilized the nitroxide radicals@US-tubes in 1% agarose gel at the same concentrations used in the suspensions experiment, the nitroxide radicals@US-tubes in 1% agarose

Table 1. Water proton relaxation properties of Tempo- and Iodo-Tempo@US-tubes and empty US-tubes in 0.17% pluronic F-108 surfactant as obtained with a Bruker Minispec (mq60) NMR spectrometer at 1.41 T (60 MHz) and 37 °C.

Sample	T_1 [ms]	T_2 [ms]	r_1 [$mM^{-1}s^{-1}$]	r_2 [$mM^{-1}s^{-1}$]	r_1/r_2
Tempo@US-tubes	3159	232	2[a)]	132[a)]	66
Iodo-Tempo@US-tubes	3278	366	2[a)]	110[a)]	55
US-tubes	2333	188	0.1[b)]	4[b)]	40
Tempo	-	-	0.15[c)]	0.10[c)]	0.7
Iodo-Tempo	-	-	0.27[c)]	0.43[c)]	1.6

Relaxivities determined from: [a)]nitroxide radical concentration by N% from elemental analysis; [b)]Ni concentration determined by ICP-OES. The relaxivities from the US-tubes represent the lowest relaxation values achieved assuming a total contribution of all the nickel paramagnetic species in the tubes; [c)]inversion recovery method and multi-echo sequence for different concentrations of the nitroxide radicals in aqueous solution.

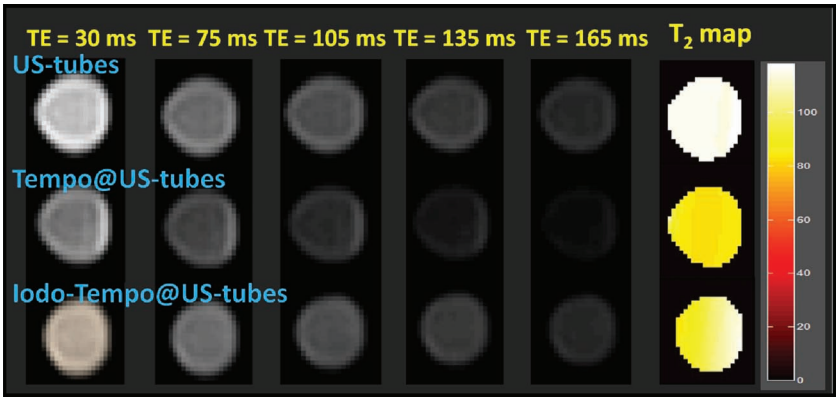

Figure 7. T_2-weighted MRI phantom images and T_2 map of the nitroxide radicals@US-tube samples and empty US-tubes in a 1% agarose gels at 3.0 T and 37 °C. The five phantoms from left to right represent the spin-echo images acquired at different echo times (TE) to measure the transverse relaxation times (T_2) of the samples. The T_2 map panel shown at the far right indicates the T_2 relaxation times (ms) in color scale.

gel showed a 2-3 fold decrease in their water proton T_2 relaxation times compared to pluronic suspensions of the nitroxide radicals@US-tube samples. The T_2 maps of the Tempo- and Iodo-Tempo@US-tubes in Figure 7 show relaxation times of 83 and 119 ms, respectively, with good contrast enhancement due to their high r_2 relaxivities. Although, the nitroxide@US-tube samples exhibit greater r_1 relaxivities in comparison with free nitroxide radicals, we did not observe significant contrast enhancement in the T_1-weighted MRI phantom images of nitroxide radicals@US-tube and empty US-tube samples at 3.0 T (Supporting Information, Figure 5S). These results suggest that the encapsulation of nitroxides within US-tubes presents a significant advantage for mainly T_2-weighted MRI compared to free nitroxides in solution.

3. Conclusions

Nitroxide radicals have been encapsulated within US-tubes. Our results suggest that the US-tubes alter the tumbling rates of the encapsulated nitroxide radicals, and therefore, their ability to induce water proton relaxation. Tempo- and Iodo-Tempo@US-tubes both demonstrate excellent relaxation rates and efficiency as T_1 and T_2 MRI CAs. T_2-weighted MRI phantom images demonstrated that the encapsulation of nitroxide radicals within the US-tubes showed good contrast enhancement due to their high r_2 relaxivities. EPR spectra of the nitroxide radicals@US-tube samples displayed characteristic signals due to the incorporation of immobilized nitroxide spin probes in the US-tubes. EPR methods are inherently more sensitive than the MRI technique; therefore, spin probes based on EPR detection could potentially offer a significant sensitivity advantage over MRI-based methods. Nitroxide radicals within US-tubes are a promising new technology for MRI, EPRI, and the measurement of oxygen concentration in vivo. Such capabilities could be useful in the diagnosis of a number of important diseases such as cancer, inflammation, and ischemia, while at the same time monitoring the effects of therapeutic treatments.

4. Experimental Section

Materials: 2,2,6,6-tetramethylpiperidine-1-oxyl (Tempo) and 4-(2-iodoacetamido)- 2,2,6,6-tetramethylpiperidine-1-oxyl (Iodo-Tempo) were obtained from Aldrich Chemical Co. and Acros Organics, respectively. Full-length SWNTs were purchased from Carbon Solutions, Inc., CA, USA. Pluronic F108 was obtained from BASF. THF was dried prior to use. All other reagents were of high purity grade and were used without further purification.

Preparation of US-Tubes: Full-length SWNTs produced by the electric-arc discharge method were cut into US-tubes by fluorination and pyrolysis at 1000 °C under argon atmosphere.[40] The cutting process reduced the amount of Ni and Y catalyst impurities (<3%), while creating defect sites in the US-tube sidewalls. The defect sites allow the loading of ions and molecules into the interior of the tubes.[28] US-tubes were purified by HCl reflux using a Soxhlet extractor with a Wilmad glass fine frit to remove amorphous carbon and remaining metal catalyst impurities, and debundled by chemical reduction using Na^0/THF to produce individualized US-tubes.[35] The US-tubes were collected by filtration, washed multiple times with deionized water, and dried at 100 °C between each of the three steps described above.

Encapsulation of Tempo and Iodo-Tempo Spin Probes into US-Tubes: Equal amounts (20 mg each) of US-tubes and nitroxide radicals were mixed together in a closed glass vessel. Sublimation of both nitroxide radicals was performed in the closed glass vessel (70 °C for 24 h), but for Iodo-Tempo it was necessary to also reduce the pressure below 300 torr. Both samples were collected by filtration and washed with abundant methanol to remove surface adsorbed nitroxide radical. The resulting Tempo- and Iodo-Tempo@US-tube samples were then dried at 60 °C.

Characterization: Thermogravimetric analysis (TGA) was performed using a TA instrument Q600. The measurements were carried out with a heating rate of 10 °C min^{-1} from 50 to 800 °C under a flow of argon (100 mL min^{-1}). X-ray photoelectron spectroscopy (XPS) and X-ray induced Auger emission analyses were performed on a PHI Quantera SXM spectrometer equipped with an Al Kα radiation source (1486.6 eV). Samples were prepared by pressing them into indium foil. Raman spectroscopy was performed using a Renishaw inVia Raman Microscope operated with a 633 nm laser and 1800 l/mm grating. ICP-OES analyses were performed by a Perkin Elmer Optima 4300 DV inductively-coupled plasma optical-emission spectrometer. Ni and Y concentrations were detected at 231.604 and 371.029 nm, respectively, while Cu (327.393 nm) was used as the internal drift standard. ICP-OES samples were prepared by digesting the US-tubes in a glass vial with 500 µL of 26% $HClO_3$ until evaporation. After the digestion procedure, samples were washed with a small amount of 2% HNO_3 to be transferred quantitatively to a 10 mL volumetric flask. Five scans were performed for each sample, and the concentration was determined from the average of scans.

EPR: Room temperature continuous wave (CW) EPR spectra were recorded on a Bruker EMX spectrometer at 9.8 GHz (X-band) using 2 mW microwave power, 1 G modulation amplitude at 100 kHz modulation frequency and a gain of 1×10^4. Spectra were recorded using 2048 point resolution with an average of ten, 200 G scans or a single 4000 G scan. The time constant was set to 20.48 ms and the conversion times were 83.89 and 163.84 ms for 200 and 4000 G sweep widths, respectively. CW EPR power saturation measurements were performed on the Tempo@US-tubes sample using powers from 0.1 to 200 mW (the gain was reduced by a factor of ten for powers between 80 and 200 mW because of detector saturation).

Proton Relaxivity Measurements: T_1 and T_2 proton relaxation times were measured using a 60 MHz Bruker Minispec (mq60) NMR spectrometer. Nitroxide radical solutions with concentrations ranging from 0.10 to 1 mM were prepared by dilution from a common stock solution. The

Tempo- and Iodo-Tempo@US-tubes were suspended with Pluronic F108 (0.17% w/v) via probe sonication for 5 min. and then centrifuged at 3,200 rpm for 10 min to remove unsuspended material. All samples were purged with nitrogen before analysis. Longitudinal (R_1) and transverse (R_2) relaxation rates in the presence of the nitroxide radicals were determined by using the inversion recovery method and spin-echo techniques. Relaxivities ($r_{1,2}$) for Tempo and Iodo-Tempo were obtained by plotting the relaxation rates as a function of the nitroxide concentrations using the relationship: $(T_{1,2}^{-1})_{obs} = (T_{1,2}^{-1})_d + r_{1,2}$ [nitroxide], where $T_{1,2obs}^{-1}$ and $T_{1,2d}^{-1}$ are the relaxation rates in s^{-1} of the sample and the medium, and [nitroxide] is the nitroxide radical concentration in mM. The slope, calculated by least squares method, represents the relaxivity due to the nitroxide radicals.

Magnetic Resonance Imaging. Proton relaxation times (T_1 and T_2 maps) of the phantom images were obtained on a clinical 3.0 T scanner (Ingenia, Philips Healthcare, Best, The Netherlands). The T_1 map was acquired using a set of inversion recovery spin-echo sequences with the following parameters: TR/TE: 9000/20 ms; a total of 11 inversion recovery images at inversion times (TI) of 100, 200, 400, 600, 800, 1000, 1500, 1800, 2200, 2500, and 3000 ms were acquired; and spatial resolution of 0.88 mm × 1.13 mm × 5.0 mm. The T_2 map was acquired from a multi-echo sequence using the following parameters: TR/TE/ΔTE: 7500/15/15 ms; a total of 16 echoes (15–240 ms) were acquired per TR at 15 ms intervals and spatial resolution of 0.88 mm × 1.13 mm × 5.0 mm. Custom-made software was used to compute the pixel-by-pixel relaxation times using MATLAB (MatWorks, Natick, MA). Both the rate decays, as well as the confidence interval limits, were estimated.

Supporting Information

Supporting Information is available from the Wiley Online Library or from the author.

Acknowledgements

The authors gratefully acknowledge the Welch Foundation (C-0627) for support of this work at Rice University.

Received: November 22, 2011
Revised: March 16, 2012
Published online: May 18, 2012

[1] P. Caravan, *Chem. Soc. Rev.* **2006**, *35*, 512.
[2] P. Caravan, J. J. Ellison, T. J. McMurry, R. B. Lauffer, *Chem. Rev.* **1999**, *99*, 2293.
[3] J. F. Keana, S. Pou, G. M. Rosen, *Magn. Reson. Med.* **1987**, *5*, 525.
[4] V. Afzal, R. C. Brasch, D. E. Nitecki, S. Wolff, *Invest. Radiol.* **1984**, *19*, 549.
[5] L. J. Berliner, H. Fujii, *Science* **1985**, *227*, 517.
[6] L. J. Berliner, H. Fujii, X.-M. Wan, S. J. Lukiewicz, *Magn. Reson. Med.* **1987**, *4*, 380.
[7] H. M. Swartz, H. Halpern, in *EPR studies of living animals and related model systems (In Vivo EPR)*, *Vol. 14* (Ed. L. J. Berliner), Kluwer Academic, New York **2002**, pp. 367–404.
[8] Z. Zhelev, R. Bakalova, I. Aoki, K.-I. Matsumoto, V. Gadjeva, K. Anzai, I. Kanno, *Mol. Pharm.* **2009**, *6*, 504.
[9] B. P. Soule, F. Hyodo, K.-I. Matsumoto, N. L. Simone, J. A. Cook, M. C. Krishna, J. B. Mitchell, *Free Radical Biol. Med.* **2007**, *42*, 1632.
[10] H. J. Halpern, *Biol. Magn. Reson.***2003**, *18*, 469.
[11] D. Citrin, A. P. Cotrim, F. Hyodo, B. J. Baum, M. C. Krishna, J. B. Mitchell, *Oncologist* **2010**, *15*, 360.
[12] R. M. Davis, S. Matsumoto, M. Bernardo, A. Sowers, K.-I. Matsumoto, M. C. Krishna, J. B. Mitchell, *Free Radical Biol. Med.* **2011**, *50*, 459.
[13] K.-I. Matsumoto, H. Yakumaru, M. Narazaki, H. Nakagawa, K. Anzai, H. Ikehira, N. Ikota, *Magn. Reson. Imaging* **2008**, *26*, 117.
[14] R. C. Brasch, M. T. McNamara, R. Ehman, W. R. Couet, T. N. Tozer, G. Sosnovsky, N. Maheswara Rao, I. Prakash, *Eur. J. Med. Chem.* **1989**, *24*, 335.
[15] P. Vallet, Y. Haverbeke, A. Bonnet, G. Subra, J.-P. Chapat, R. N. Muller, *Magn. Reson. Med.* **1994**, *32*, 11.
[16] G. Likhtenshtein, J. Yamauchi, S. Nakatsuji, A. I. Smirnov, R. Tamura, *Nitroxides: Applications in Chemistry, Biomedicine, and Materials Science*, Wiley-VCH, Weinheim **2008**.
[17] J. F. Keana, S. Pou, *Physiol. Chem. Phys. Med. NMR* **1985**, *17*, 235.
[18] H. F. Bennett, R. D. Brown, S. H. Koenig, H. M. Swartz, *Magn. Reson. Med.* **1987**, *4*, 93.
[19] A. Olankitwanit, V. Kathirvelu, S. Rajca, G. R. Eaton, S. S. Eaton, A. Rajca, *Chem. Commun.* **2011**, *47*, 6443.
[20] H. Hayashi, S. Karasawa, A. Tanaka, K. Odoi, K. Chimaka, H. Kuribayashi, N. Koga, *Magn. Reson. Chem.* **2009**, *47*, 201.
[21] M. Gussoni, F. Greco, P. Ferruti, R. Elisabetta, A. Ponti, L. Zetta, *New J. Chem.* **2008**, *32*, 323.
[22] Y. Huang, A. Nan, G. M. Rosen, C. S. Winalski, E. Schneider, P. Tsai, H. Ghandehari, *Macromol. Biosci.* **2003**, *3*, 647.
[23] C. S. Winalski, S. Shortkroff, E. Schneider, H. Yoshioka, R. V. Mulkern, G. M. Rosen, *Osteoarthritis Cartilage* **2008**, *16*, 815.
[24] C. S. Winalski, S. Shortkroff, R. V. Mulkern, E. Schneider, G. M. Rosen, *Magn. Reson. Med.* **2002**, *48*, 965.
[25] Y. Sato, H. Hayashi, M. Okazaki, M. Aso, S. Karasawa, S. Ueki, H. Suemune, N. Koga, *Magn. Reson. Chem.* **2008**, *46*, 1055.
[26] S. R. Burks, E. D. Barth, H. J. Halpern, G. M. Rosen, J. Kao, *Biochim. Biophys. Acta.* **2009**, *1788*, 2301.
[27] H.-C. Chan, K. Sun, R. Magin, H. M. Swartz, *Bioconjugate Chem.* **1990**, *1*, 32.
[28] B. Sitharaman, K. Kisell, K. B. Hartman, L. Tran, A. Baikalov, I. Rusakova, Y. Sun, H. A. Khant, S. J. Ludtke, W. Chiu, S. Laus, E. Tóth, L. Helm, A. E. Merbach, L. J. Wilson, *Chem. Commun.* **2005**, 3915.
[29] J. M. Schnorr, T. M. Swager, *Chem. Mater.* **2011**, *23*, 646.
[30] H.-C. Wu, X. Chang, L. Liu, F. Zhao, Y. Zhao, *J. Mater. Chem.* **2010**, *20*, 1036.
[31] S. Campestrini, C. Corvaja, M. De Nardi, C. Ducati, L. Franco, M. Maggini, M. Meneghetti, E. Menna, G. Ruaro, *Small* **2008**, *4*, 350.
[32] A. K. Dhami, S. Bhat, A. Sharma, S. V. Bhat, *Spectrochim. Acta A* **2008**, *69*, 1178.
[33] Y. Mackeyev, K. B. Hartman, J. S. Ananta, A. Lee, L. J. Wilson, *J. Am. Chem. Soc.* **2009**, *131*, 8342.
[34] A. A. Hassan, B. T.-Y. Chan, L. Tran, K. B. Hartman, J. S. Ananta, Y. Mackeyev, L. Hu, R. G. Pautler, L. J. Wilson, A. V. Lee, *Contrast Media Mol. Imaging.* **2010**, *5*, 34.
[35] J. M. Ashcroft, K. B. Hartman, Y. Mackeyev, C. Hofmann, S. Pheasant, L. B. Alemany, L. J. Wilson, *Nanotechnology* **2006**, *17*, 5033.
[36] A. Guven, I. Rusakova, M. T. Lewis, L. J. Wilson, *Biomaterials* **2011**, *33*, 1455.
[37] J. M. Ashcroft, K. B. Hartman, K. Kisell, Y. Mackeyev, S. Pheasant, S. Young, P. Van der Heide, A. Mikos, L. J. Wilson, *Adv. Mater.* **2007***19*, 573.
[38] K. B. Hartman, D. K. Hamlin, D. S. Wilbur, L. J. Wilson, *Small* **2007**, *3*, 1496.
[39] L. Tran, R. Krishnamurthy, R. Muthupillai, M. Cabreira-Hansen, J. T. Willerson, E. C. Perin, L. J. Wilson, *Biomaterials* **2010**, *31*, 9482.
[40] Z. Gu, H. Peng, R. H. Hauge, R. E. Smalley, J. L. Margrave, *Nano Lett.* **2002**, *2*, 1009.
[41] Y. Ma, C. Loyns, P. Price, V. Chechik, *Org. Biomol. Chem.* **2011**, *9*, 5573.

[42] B. A. Howell, I. Q. Li, P. B. Priddy, A. Ellaboudy, *Thermochim. Acta* **1999**, *340–341*, 279.
[43] K. Kisell, K. B. Hartman, P. Van der Heide, L. J. Wilson, *J. Phys. Chem. B* **2006**, *110*, 17425.
[44] C. Journet, W. K. Maser, P. Bernier, A. Loiseau, M. Lamy de la Chapelle, S. Lefrant, P. Deniard, R. Lee, J. E. Fisher, *Nature* **1997**, *388*, 756.
[45] K. Yanagi, K. Iakoubovskii, H. Matsui, H. Matsuzaki, H. Okamoto, Y. Miyata, S. Kazaoui, N. Minami, H. Kataura, *J. Am. Chem. Soc.* **2007**, *129*, 4992.
[46] T. Takenobu, T. Takano, M. Shiraishi, Y. Murakami, M. Ata, H. Kataura, Y. Achiba, Y. Iwasa, *Nat. Mater.* **2003**, *2*, 683.
[47] M. Zaka, Y. Ito, H. Wang, W. Yan, A. Robertson, Y. A. Wu, M. H. Rummeli, D. Staunton, T. Hashimoto, J. J. L. Morton, A. Ardavan, G. A. Briggs, J. H. Warner, *ACS Nano* **2010**, *4*, 7708.
[48] A. A. Konchits, F. V. Motsnyi, Y. N. Petrov, S. P. Kolesnik, V. S. Yefanov, M. L. Terranova, E. Tamburri, S. Orlanducci, V. Sessa, M. Rossi, *J. Appl. Phys.* **2006**, *100*, 124315.
[49] K. Shen, D. L. Tierney, T. Pietra, *Phys. Rev. B* **2003**, *68*, 165418.
[50] L. H. Piette, J. C. Hsia, *Spin labeling II: Theory and Applications*, Academic Press, New York **1979**.
[51] F. Radner, C. J. Hersvall, A. Rassat, J.-H. Ardenkjaer-Larsen, S. Gambarelli, D. Jaquen, *Res. Chem. Intermed.* **1996**, *22*, 417.
[52] J. S. Ananta, B. Godin, R. Sethi, L. Moriggi, X. Liu, R. Serda, R. Krishnamurthy, R. D. Bolskar, L. Helm, M. Ferrari, L. J. Wilson, P. Decuzzi, *Nat. Nanotechnol.* **2010**, *5*, 815.
[53] D. Cheng, G. Hong, W. Wang, R. Yuan, H. Ai, J. Shen, B. Liang, J. Gao, X. Shuai, *J. Mater. Chem.* **2011**, *21*, 4796.
[54] M. D. Mitchell, L. Harold, L. Axel, P. M. Joseph, *Magn. Reson. Imaging.* **1986**, *4*, 263.